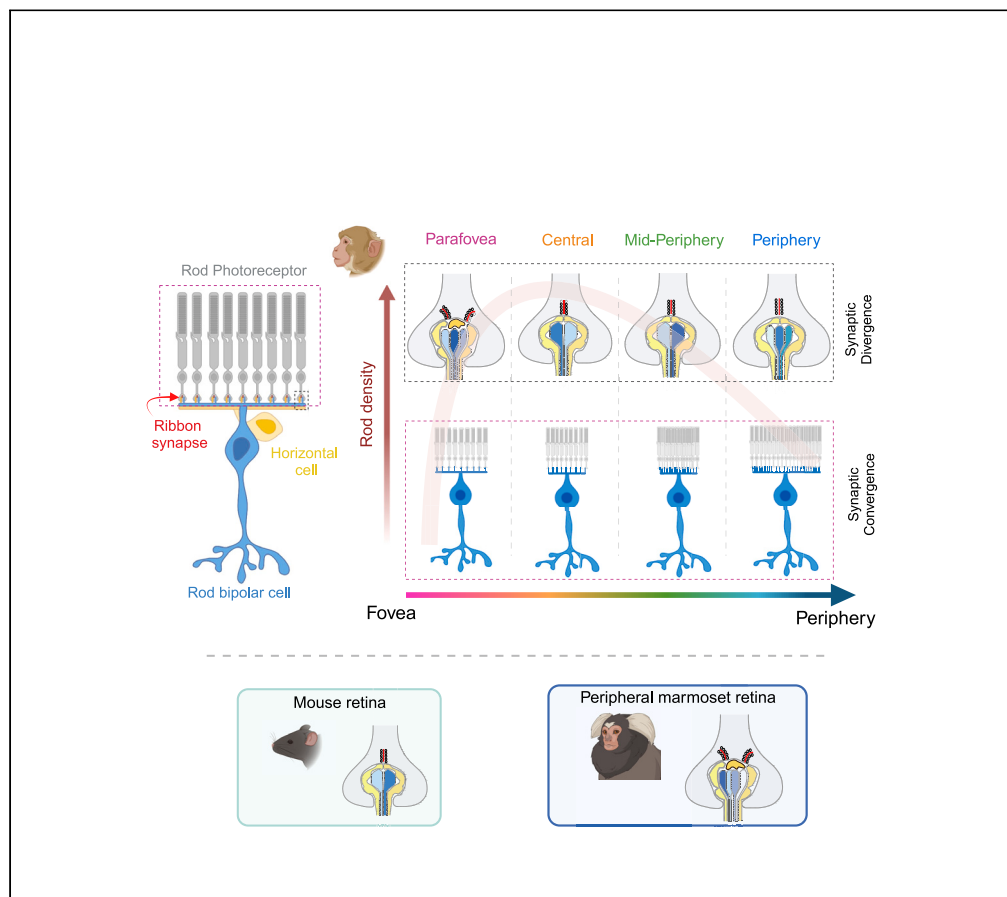


Article

Regional variation in the organization and connectivity of the first synapse in the primate night vision pathway



Aindrila Saha, Juan Zuniga, Kainat Mian, Haoshen Zhai, Paul J. Derr, Mrinalini Hoon, Raunak Sinha

mhoon@wisc.edu (M.H.)
raunak.sinha@wisc.edu (R.S.)

Highlights

Primate rod photoreceptor synapse exhibits regional differences in organization

Numbers of ribbons and postsynaptic partners in the rod synapse vary across regions

Synaptic convergence of rods changes in a non-graded manner across regions

Regional changes in photoreceptor density drive changes in rod synapse organization

Saha et al., iScience 26, 108113
November 17, 2023 © 2023 The Author(s).
<https://doi.org/10.1016/j.isci.2023.108113>

Article

Regional variation in the organization and connectivity of the first synapse in the primate night vision pathway

Aindrila Saha,^{1,2,4} Juan Zuniga,^{1,4} Kainat Mian,^{1,4} Haoshen Zhai,¹ Paul J. Derr,¹ Mrinalini Hoon,^{1,2,3,*} and Raunak Sinha^{1,2,3,5,*}

SUMMARY

Sensitivity of primate daylight vision varies across the visual field. This is attributed to regional variations in cone photoreceptor density and synaptic connectivity of the underlying circuitry. In contrast, we have limited understanding of how synapse organization of the primate night vision pathway changes across space. Using serial electron microscopy, we reconstructed the first synapse of the night vision pathway between rod photoreceptors and second-order neurons, at multiple locations from the central part of the primate retina, fovea, to the periphery. We find that most facets of the rod synapse connectivity vary across retinal regions. However, rod synaptic divergence and convergence patterns do not change in the same manner across locations. Moreover, patterns of rod synapse organization are tightly correlated with photoreceptor density. Such regional heterogeneities revise the connectivity diagram of the primate rod synapse which will shape synapse function and sensitivity of the night vision pathway across visual space.

INTRODUCTION

Humans like most other primates do not sample the visual scene uniformly across space and as a result exhibit remarkable differences in sensitivity between central and peripheral vision.^{1–3} This is largely driven by regional differences in the packing density of photoreceptors and the underlying primate retinal circuitry.^{4–6} Cone photoreceptors drive daylight and rod photoreceptors mediate night vision. We know a great deal about how regional changes in cone photoreceptor density result in variations in the overall structure and connectivity of the cone-driven neural circuits at distinct locations in the primate retina.^{6–8} However, our understanding of how the basic architecture of the first visual synapse for the rod photoreceptor-driven night vision pathway as well as the connectivity pattern of the rod photoreceptor output synapses to second-order neurons, rod bipolar cells (RBCs), and horizontal cells (HCs) (Figure 1A) changes between retinal regions remains far from complete. This is of particular importance because the primate retina is heterogeneous across locations and as such extrapolation of neural connectivity across regions is not possible. Like humans, a hallmark of the retina in diurnal primates is the presence of an anatomical specialization called the fovea, which accounts for over half of the retinal output to the rest of the brain.⁴ The presence of the fovea creates a topographic variation in the density of rods, cones, their relative ratio, and the density of subsequent postsynaptic neurons from the fovea to the peripheral primate retina.^{5,9,10} Previous studies have shown that the number of synapses made by individual cone photoreceptors is almost 2-fold lower in the fovea than in the peripheral primate retina.¹¹ In addition, the synaptic connectivity of cones to downstream neurons in the dominant neural circuit of the fovea, the midget pathway, changes significantly across locations.^{6,7} Our focus in this study is to provide a similar understanding for the number, organization, and connectivity of the rod photoreceptor synapse and the primary night vision pathway across retinal locations in primates.

Rod and cone photoreceptors form specialized invaginating synapses with a stereotypic organization conserved among mammals.^{9,12–15} This synapse is commonly referred to as a “triad” synapse based on its initial characterization at the cone axon terminals which include a presynaptic vesicle anchoring structure, the ribbon, juxtaposed to three distinct postsynaptic elements, one provided by BCs and two from HCs^{13,14,16} (Figure 1A). Unlike conventional synapses in the brain, where neurotransmitter release is intermittent, ribbons allow the photoreceptor synapses to tether a large number of synaptic vesicles near the release site for a high rate of tonic neurotransmitter release in darkness.^{17–19} Light inputs are encoded via graded changes in this tonic rate of transmitter release. A previous study on cat retina suggested that the presence of a single large crescent-shaped ribbon which forms a single release site, called active zone, in rod terminals makes them unique compared to all other mammalian neurons with several active zones.¹⁸ This idea of a single active zone per rod terminal was revised by subsequent studies, which reported that a single ribbon typically has two distinct active zones which are defined as two distinct “synaptic

¹Department of Neuroscience, University of Wisconsin, Madison, WI, USA

²McPherson Eye Research Institute, University of Wisconsin, Madison, WI, USA

³Department of Ophthalmology and Visual Sciences, University of Wisconsin, Madison, WI, USA

⁴These authors contributed equally

⁵Lead contact

*Correspondence: mhoon@wisc.edu (M.H.), raunak.sinha@wisc.edu (R.S.)

<https://doi.org/10.1016/j.isci.2023.108113>



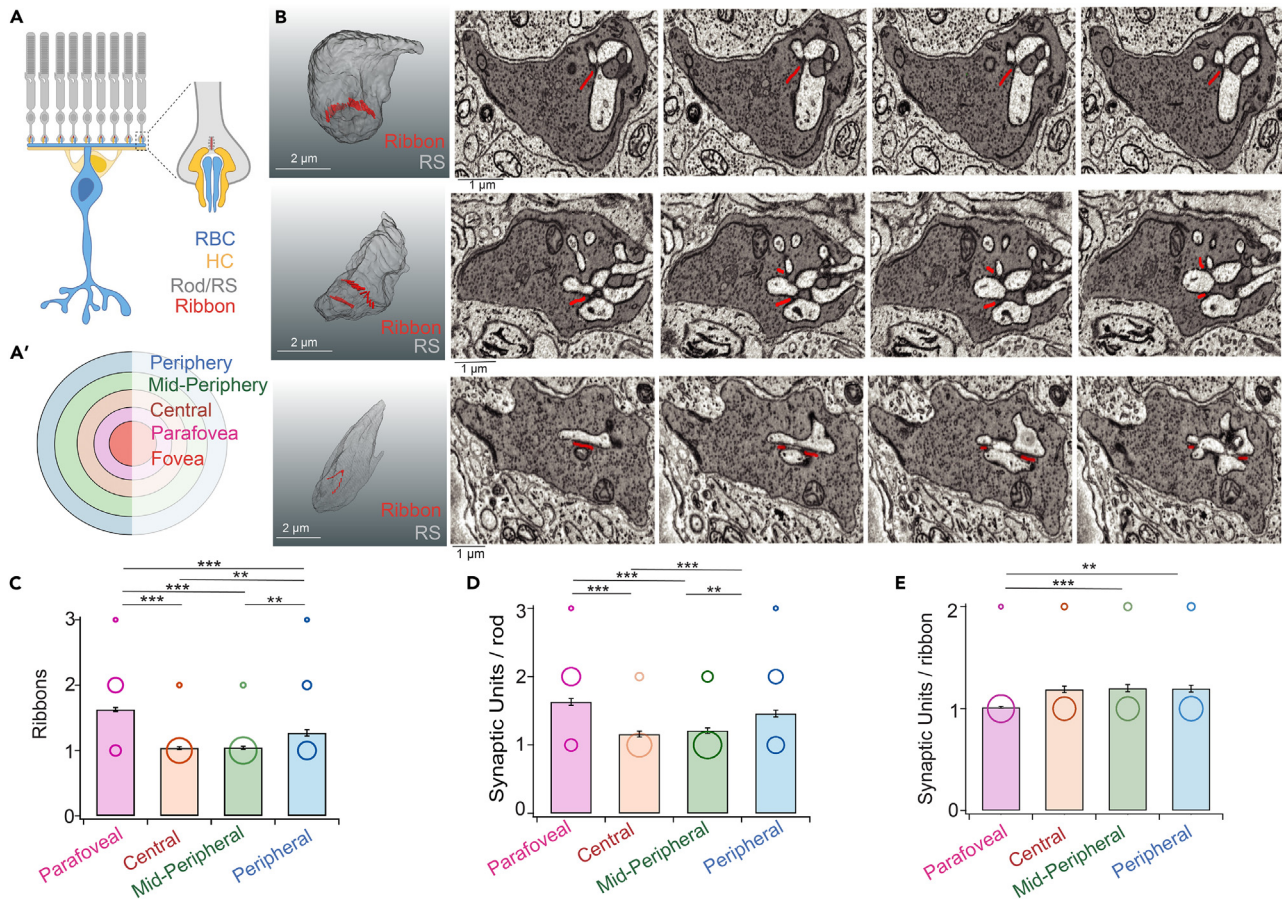


Figure 1. Rod synapse organization across locations in primate macaque retina

(A) Schematic representation of the rod to rod bipolar cell (RBC) ribbon synapse in the mammalian retina. Each RBC pools inputs from multiple photoreceptors. The signal from the rod photoreceptors is modified by input from horizontal cell (HC) processes. Inset: Schematic of a rod terminal (rod spherule or RS) demonstrating a classical ribbon synapse flanked by two central RBC processes and two lateral HC processes. (A') Schematic representation of the different regions of the macaque retina.

(B) 3D rendering of a macaque rod spherule (gray) with one ribbon (red) (*top-left*); 2 ribbons (*middle-left*), and one ribbon forming two synaptic units by contacting two distinct sets of postsynaptic partners (*bottom-left*). Corresponding single-plane annotated EM images displaying the spherules and their ribbon synapses as seen during reconstructions. Four consecutive images depicted for each scenario (*right panels*).

(C) Number of ribbons per individual rod spherule for all four regions of interest (parafovea, central, mid-periphery, and periphery) in the macaque retina. Parafovea: 1.63 ± 0.03 ($n = 88$), central: 1.05 ± 0.02 ($n = 93$), mid-periphery: 1.05 ± 0.02 ($n = 117$), and periphery: 1.27 ± 0.05 ($n = 92$). n = number of rod spherules reconstructed. The size of the circle represents the relative frequency of occurrence of rod spherules containing 1, 2, or 3 ribbons with respect to the total number of rod spherules in a specific region (see [Table S1](#) and [STAR methods](#)). Error bars represent mean \pm SEM. Statistics: Tukey's multiple comparison test was performed.

(D) Number of synaptic units per rod spherule across the four regions of interest. Parafovea: 1.65 ± 0.05 ($n = 88$), central: 1.16 ± 0.04 ($n = 93$), mid-periphery: 1.21 ± 0.04 ($n = 117$), and periphery: 1.46 ± 0.05 ($n = 92$). n = number of rod spherules reconstructed. The size of the circle represents the relative frequency of occurrence of rod spherules containing 1, 2, or 3 synaptic units with respect to the total number of rod spherules in a specific region (see [Table S1](#) and [STAR methods](#)). Error bars represent mean \pm SEM. Statistics: Tukey's multiple comparison test was performed.

(E) Number of synaptic units per ribbon in each rod spherule across the four regions of interest. Parafovea: 1.01 ± 0.01 ($n = 143$), central: 1.1 ± 0.03 ($n = 98$), mid-periphery: 1.17 ± 0.04 ($n = 121$), and periphery: 1.16 ± 0.03 ($n = 116$). n represents the number of ribbon synapses documented at each region. The size of the circle represents the relative frequency of occurrence of ribbon synapses containing 1 or 2 synaptic units with respect to the total number of ribbon synapses in a specific region (see [Table S1](#) and [STAR methods](#)). Error bars represent mean \pm SEM. Statistics: Tukey's multiple comparison test was performed.

units" each consisting of a ribbon or part of a ribbon opposed to non-overlapping postsynaptic processes.^{20,21} Such a specialized presynaptic design was thought to mediate the high baseline rate of neurotransmitter release from rod terminals in darkness.²⁰ It remains largely unknown, however, whether such a precise architecture of the rod synapse, including the number of ribbons and synaptic units, remains invariant or changes across locations within the primate retina. In fact, a conclusive study with a systematic comparison of rod synapse ultrastructure and the precise pattern of synaptic connectivity between rods and the second-order neurons across multiple locations within the same primate retina is missing.

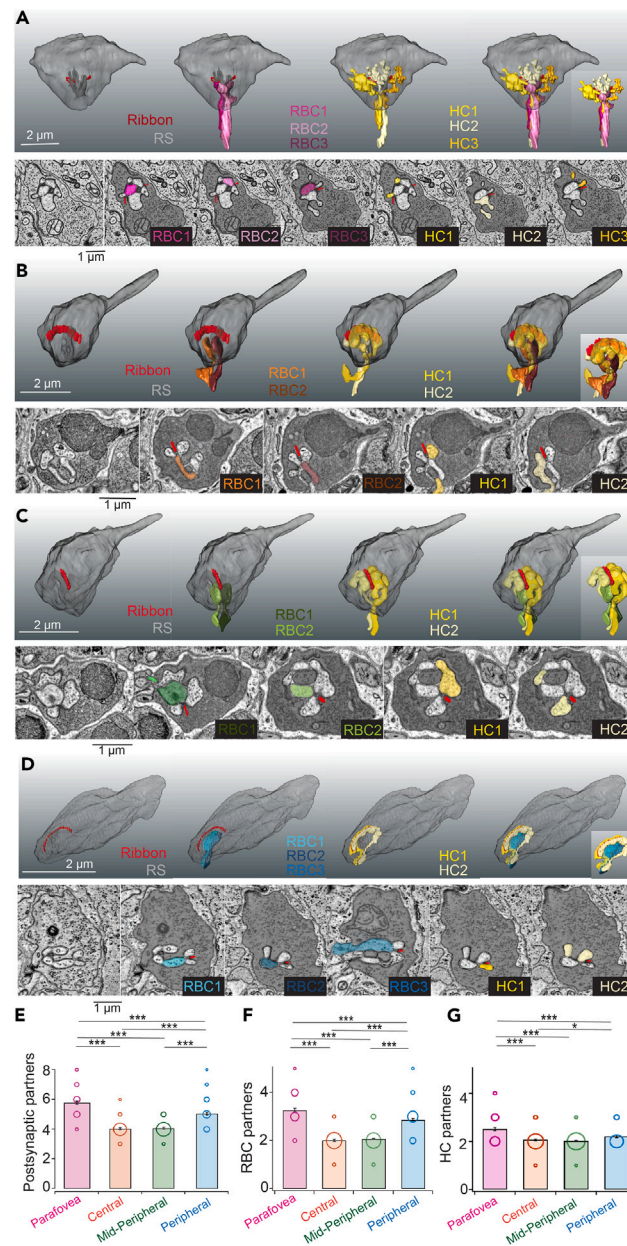


Figure 2. Synaptic divergence at the rod synapse across retinal eccentricity

(A) 3D rendering of a parafoveal rod spherule (RS) with 2 ribbons contacting 3 RBC (RBC1-3) and 3 HC (HC1-3) partners. The top panel shows the 3D reconstructed image whereas the bottom panel shows annotated single-plane images of invaginating contact with the different postsynaptic partners. The image on the extreme left is an example raw image of the terminal. Typically, parafoveal rods contact 6 postsynaptic partners and contain two ribbons. Scale bar: 1 μm for single-plane images and 2 μm for 3D renderings.

(B) 3D rendering of a central rod spherule with 1 ribbon contacting 2 RBC (RBC1-2) and 2 HC (HC1-2) partners. The top panel shows the 3D reconstructed image whereas the bottom panel shows annotated single-plane images of invaginating contact with the different postsynaptic partners. The image on the extreme left is an example raw image of the terminal. Typically, central rods utilize a single ribbon to connect with 4 postsynaptic partners.

(C) 3D rendering of a mid-peripheral rod spherule with a single ribbon contacting 2 RBC (RBC1-2) and 2 HC (HC1-2) partners. The top panel shows the 3D reconstructed image whereas the bottom panel shows annotated single-plane images of invaginating contact with the different postsynaptic partners. The image on the extreme left is an example raw image of the terminal. Typically, mid-peripheral rods utilize a single ribbon to connect with 4 postsynaptic partners.

(D) 3D rendering of a peripheral rod spherule containing 1 ribbon apposed to 3 RBC (RBC1-3) and 2 HC (HC1-2) partners. The top panel shows the 3D reconstructed image whereas the bottom panel shows annotated single-plane images of invaginating contact with the different postsynaptic partners. The image on the extreme left is an example raw image of the terminal. Typically, peripheral rod spherules contact 5 postsynaptic partners at one ribbon.

Figure 2. Continued

(E) Total number of postsynaptic partners (RBC+HC) contacting a rod spherule across eccentricities. The bar represents the average with the different sized circles representing the number of instances of each occurrence. Parafovea: 5.81 ± 0.11 ($n = 88$), central: 4.03 ± 0.07 ($n = 104$), mid-periphery: 4.13 ± 0.05 ($n = 117$), and periphery: 5.03 ± 0.09 ($n = 92$). In this plot and in plots shown in panel F and G, the size of the circle represents the relative frequency of occurrence of rod spherules containing the different numbers of postsynaptic partners with respect to the total number of rod spherules (see Table S2 and STAR methods). n represents number of rod spherules. Error bars represents mean \pm SEM. Statistics: Tukey's multiple comparison test was performed.

(F and G) Number of RBCs (F) and HCs (G) contacting a rod spherule across different regions of the macaque retina. Number of RBCs in (F) - Parafovea: 3.3 ± 0.07 ($n = 88$), central: 2 ± 0.04 ($n = 104$), mid-periphery: 2.11 ± 0.04 ($n = 117$), and periphery: 2.84 ± 0.07 ($n = 92$). Number of HCs in (G) - Parafovea: 2.51 ± 0.07 ($n = 88$), central: 2.06 ± 0.04 ($N = 104$), mid-periphery: 2.02 ± 0.02 ($n = 117$), and periphery: 2.2 ± 0.04 ($n = 92$). n represents number of rod spherules. Error bars represents mean \pm SEM. Statistics: Tukey's multiple comparison test was performed.

To assess how the rod photoreceptor synapse and its connectivity with postsynaptic partners change across locations in the primate retina, we used serial block-face scanning electron microscopy (SBEM) to image and reconstruct the rod, RBC, and HC circuitry at four distinct locations in the macaque outer retina—parafoveal (~ 1 mm from the foveal center), central (~ 3 mm), mid-peripheral (~ 5 mm), and far peripheral (~ 10 mm) retina (Figure 1A'). We find that not only does the number of ribbon synapses per rod axon terminal change across eccentricities but the fundamental organization of the rod synapse also varies across locations. We also discovered that basic properties of synaptic divergence and convergence of rod to RBC and HC connectivity change in a nonlinear manner with increasing distance from the fovea. To further determine if these differences in the organization of the rod synapse are dependent on the relative differences in the rod and cone density across locations, we compared reconstructions of the rod to RBC, HC synaptic circuitry in the rod-abundant mouse retina with a high rod-to-cone ratio vs. reconstructions in the cone-abundant peripheral retina of marmosets where the rod-to-cone ratio is low and comparable to that of the macaque parafovea^{9,22,23} (Figure S1). Our results across retinal locations and species indicate that the configuration and connectivity of the rod synapse depend on the relative packing of rods and cones across the photoreceptor sheet of the primate retina. These new insights into the regional variation of synapse organization and wiring of the rod to postsynaptic RBCs and HCs have important functional and perceptual implications in how the dim light sensitivity of the primate night vision pathway is tuned across the visual field.

RESULTS

The number and organization of rod ribbon synapses vary across retinal locations

In the primate retina there is a pronounced regional increase in the density of both rods and RBCs from the fovea which reaches peak density at ~ 15 degrees of visual angle, which corresponds to ~ 4 mm from the foveal center in macaque retina, followed by a gradual decrease farther in the peripheral retina^{4,5,9,10} (Figure S1A). We verified this regional heterogeneity in rod density by quantifying the density of rod terminals in our electron microscopy (EM) stack across regions, since the entire outer nuclear layer was not always present in the image stack (Figure S1C). Thus far, there is sparse evidence which suggests that the number of synapses between rods and its postsynaptic partners vary across retinal locations.^{20,24} Our SBEM reconstructions across four retinal locations of the macaque retina showed the stereotypical invaginating configuration of the synapse between rod axon terminals, called spherules, and the processes of the RBCs and HCs (Figure 1B). RBC dendrites make invaginating contacts at rod spherules forming the central element in the synaptic triad, and HC processes form the lateral elements (Figure 1B). Rods across species have typically been shown to consist of 1–2 ribbons in their axon terminals.^{20,21} We reconstructed ~ 400 primate rod spherules across the four retinal locations and found significant differences in rod ribbon numbers and synapse organization across eccentricity (Figure 1). We find that parafoveal rods have the lowest instances of single ribbon per rod spherule unlike peripheral, mid-peripheral, and central rods where most of the rods contained a single ribbon. In fact, rod spherules with two or more ribbons were most common in the parafovea and quite rare in the other locations. Thus, on average, parafoveal rods contain the highest number of ribbons followed by the peripheral, mid-peripheral, and central rods (Figure 1C; Table S1). We next estimated the length of the ribbons at each of the four locations (Figure S2), which did not exhibit remarkable changes between locations even though the parafoveal rods seem to have slightly smaller ribbons and the peripheral rods seem to have comparatively larger ribbons.

A central feature of the rod ribbon organization is a synaptic unit comprising a ribbon or part of a ribbon juxtaposed to a pair of lateral elements and one or more central elements (Figure 1B; see STAR methods). Each ribbon can have one (Figure 1B, top and middle panel) or two synaptic units (Figure 1B, bottom panel). In the latter scenario, a single ribbon is opposed to two sets of lateral and central elements at two distinct regions of the ribbon with at least one non-overlapping partner (Figure 1B, bottom panel). Previous work has shown that primate rod photoreceptors in general have two synaptic units per spherule.^{20,21} Here we determined the organization of ribbon output sites within rod spherules across locations, categorizing the number of associated synaptic units. We find that the numerically dominant configuration in rod spherules is one synaptic unit per ribbon across all locations (Figures 1C–1E). There are however some instances of two synaptic units per ribbon which are relatively higher in occurrence in the central and peripheral locations than in the parafovea (Figure 1E; Table S1). When we compare the number of synaptic units per rod spherule, we find that whereas the central, mid-peripheral, and peripheral rods primarily demonstrate one synaptic unit per spherule, the parafoveal rods have significantly higher instances of two synaptic units per rod spherule (Figure 1D; Table S1). The organization and number of ribbons for central and mid-peripheral rods were more similar compared to the other two locations, i.e., parafoveal and peripheral retina. This pattern is also consistent with the reduced rod density in the periphery and the parafovea compared to the central retina (Figure S1), thereby allowing greater space for packing the rod spherules. Altogether, these findings indicate key differences in the organization of the rod spherule ribbon synapses across locations in the primate retina.

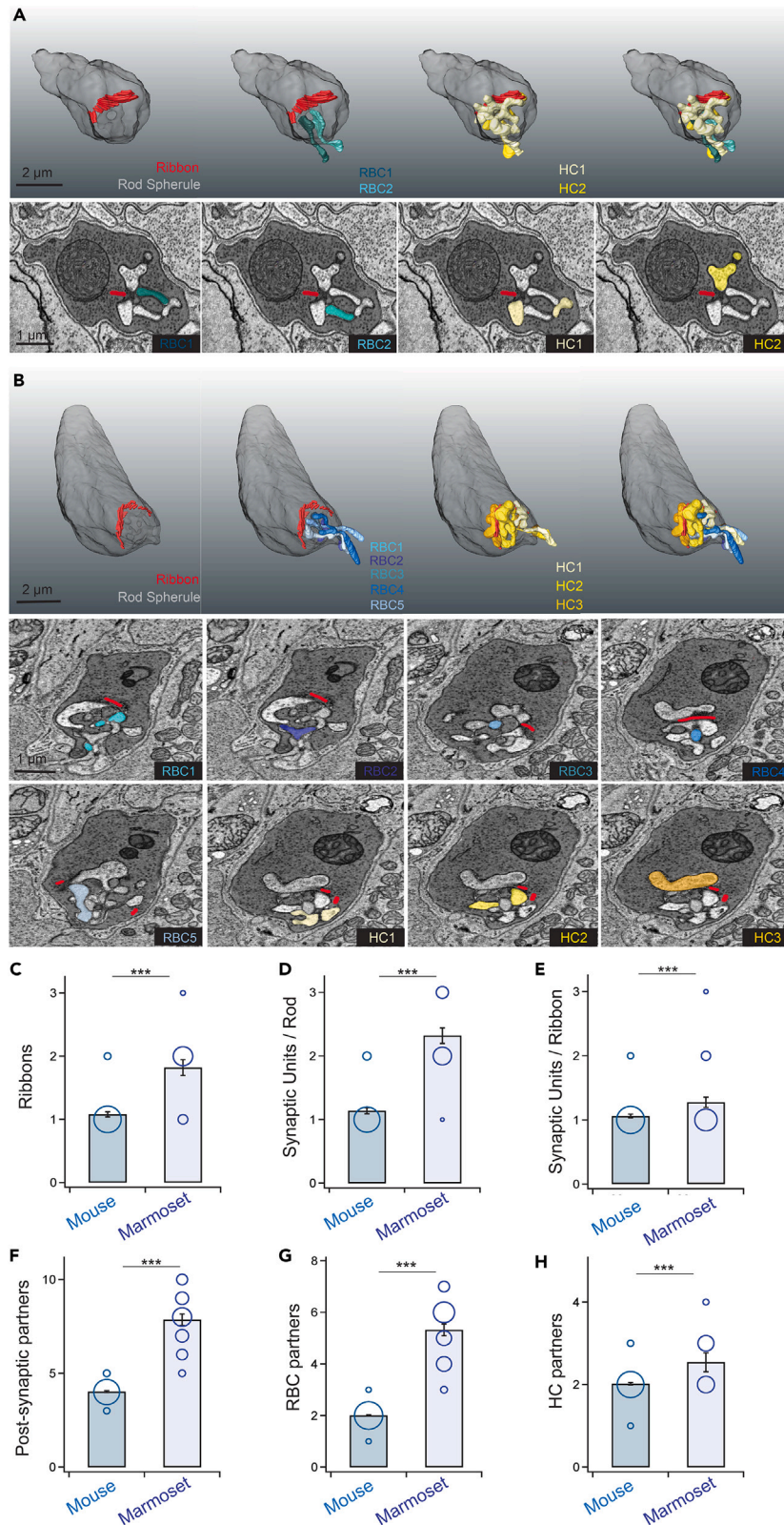


Figure 3. Synapse organization and divergence at rod photoreceptors in mouse and marmoset retina

(A and B) 3D rendering of typical organization of the rod terminal ribbon synapse and apposed postsynaptic partners in mouse (A, top) and marmoset (B, top) rod axon terminals. Mouse rods typically have 4 postsynaptic partners (2 RBCs and 2 HCs) whereas marmoset rods have significantly higher degree of synaptic divergence with the most common configuration of ~8 postsynaptic partners (typically 5 RBCs and 3 HCs). Bottom panel (A and B) depicts corresponding single-plane annotated images depicting invaginating contact of each postsynaptic partner at the rod spherule.

(C–H) Quantification of the number of ribbons per rod spherule Mouse: 1.08 ± 0.04 (n = 50), Marmoset: 1.82 ± 0.125 (n = 22) (C), number of synaptic units per rod spherule Mouse: 1.14 ± 0.05 (n = 50), Marmoset: 2.32 ± 0.12 (n = 22) (D), number of synaptic units per rod ribbon Mouse: 1.06 ± 0.03 (n = 54), Marmoset: 1.28 ± 0.08 (n = 40) (E), number of total postsynaptic partners contacting a rod spherule Mouse: 4.02 ± 0.05 (n = 50), Marmoset: 7.86 ± 0.3 (n = 22) (F), number of RBC partners contacting a rod spherule Mouse: 2.02 ± 0.04 (n = 50), Marmoset: 5.32 ± 0.13 (n = 22) (G) and number of HC partners contacting a rod spherule (H) for mouse vs. marmoset rod spherules Mouse: 2 ± 0.04 (n = 50), Marmoset: 2.55 ± 0.13 (n = 22). The size of the circle represents the relative frequency of occurrence as plotted in Figures 1 and 2 (see Table S3, STAR methods). Scale bar: 1 μ m for single-plane images and 2 μ m for 3D renderings. n = number of rod spherules reconstructed. Error bars represents mean \pm SEM. Statistics: An unpaired, two-tailed student's t test was performed.

Divergence from the rod photoreceptor synapse varies across retinal eccentricity

A common pattern of synapse organization in the nervous system is synaptic divergence where a single presynaptic neuron makes output synapses onto multiple postsynaptic partners.^{25–28} In the retina, synaptic divergence is exemplified at photoreceptor synapses.^{29–32} The extent of synaptic divergence from rods to downstream RBC and HC neurites varies across species.^{15,16,20} For instance, the number of RBC central elements per rod spherule can vary from one to five and the number of HC lateral elements per rod spherule can vary from two to four in primate retina.^{20,24} To assess how synaptic divergence varies across retinal space in the macaque retina, we reconstructed all the RBC and HC neurites that enter the rod spherule and are postsynaptically localized at the ~400 rod spherules across four retinal locations. We counted the number of RBC and HC processes contacting each rod spherule (Figures 2A–2G). Our results show that on average, rods in the macaque retina irrespective of their retinal location make synaptic contacts with more than one RBC central element. Parafoveal rods have the highest number of postsynaptic RBC central elements followed by the peripheral rods. Central and mid-peripheral rods have the lowest number of postsynaptic RBC central elements (Figure 2F). 47% of the parafoveal rods connect to three distinct RBCs; 40% of them have four invaginating RBCs, whereas 60% of the rods in the peripheral retina diverge their signals onto three RBCs. This higher degree of divergence is unique to the parafoveal and peripheral retina, as in the central and mid-peripheral retina, >75% of the rods have only two RBC partners invaginating into their axon terminals (Table S2).

We find that parafoveal rods also make synaptic contacts with the highest number of HC processes compared to rods in other locations. In fact, 38% of the parafoveal rods make synaptic contacts with three HC lateral elements, whereas a large population (>80%) of rods at other regions contact only two HC lateral elements much like in cat retina¹⁸ (Table S2). Our findings thus reveal that rods in the parafovea have the greatest number of postsynaptic partners, i.e., exhibit the greatest extent/degree of synaptic divergence. Furthermore, this synaptic divergence from the rod spherule varies remarkably with location in the macaque retina (Figure 2E). Besides differences in the average number of rod postsynaptic partners across locations, we also found a great degree of variability and hence a broad distribution of the number of postsynaptic partners in the parafoveal and peripheral rods—ranging from 4 to 8 partners. In contrast, central and mid-peripheral rods had a more conserved organization of postsynaptic partners varying between 3 and 6 partners with a narrow distribution that peaks at four (Figure 2E; Table S2; Figure S3). The higher number of postsynaptic divergences at parafoveal and peripheral primate rods may be shaped by space constraints in the primate retina due to lower rod density and consequently lower density of RBCs in these locations.²⁴ Taken together, our results indicate that the greatest degree of signal divergence from the first synapse of the night vision pathway is found in the parafoveal macaque retina.

Rod synapse organization and divergence in mouse vs. marmoset retina

If the regional differences that we observed in the number of ribbon synapses per rod spherule and rod synaptic divergence are in fact due to changes in the relative density of rod to cone photoreceptors in macaque retina, then we predict that we should see similar differences in synapse arrangement between animal species where the retina has an abundance of rods vs. cones. To test this prediction, we performed SBEM and reconstructed the rod synapse and its postsynaptic connections with RBCs and HCs in the mouse retina which has a very high density of rods relative to cones, ~32:1,²² and contrasted that with rod synapse organization in the marmoset peripheral retina which has a much lower rod-to-cone density, ~4:1, similar to the distribution in the macaque parafovea.^{9,23} The rod to RBC, HC synapse in the mouse retina displays a stereotypic organization where a single presynaptic ribbon is juxtaposed to two HC lateral elements and two RBC central elements forming a tetrad^{15,20} and a single synaptic unit (Figure 3A). This is the dominant pattern of rod synapse connectivity in the mouse retina with relatively few instances of rod spherules with two ribbons or two synaptic units per ribbon (Figures 3C–3E). There are also rare instances of three or five postsynaptic processes in the mouse rod spherule (Figures 3F–3H). Overall, the pattern of rod synaptic connections in mouse retina is consistent with previous findings^{15,21} and is also similar to observations in central and mid-peripheral macaque retina (Figures 2E–2G). In contrast, rod synapses in the marmoset peripheral retina exhibit striking differences both in their architecture and connectivity with the postsynaptic RBC and HC partners compared to mouse and macaque retina (Figure 3B). Most of the rod spherules in marmoset retina contain 2 ribbons with 1–2 synaptic units per ribbon resulting in a total of 2–3 synaptic units per rod terminal (Figures 3C–3E; Table S3). The length of the ribbon in both mouse and marmoset retina is similar to that in macaque retina (Figure S2) and consistent with previous estimates in mouse retina.^{33,34} Increased number of ribbons per rod terminal results in an increased number of postsynaptic partners and an increased diversity in the pattern of connectivity. Unlike the mouse rod terminal, the number of postsynaptic processes for a given marmoset rod terminal exhibits a broad distribution ranging from 5 to 10 with the most frequent instances of 8

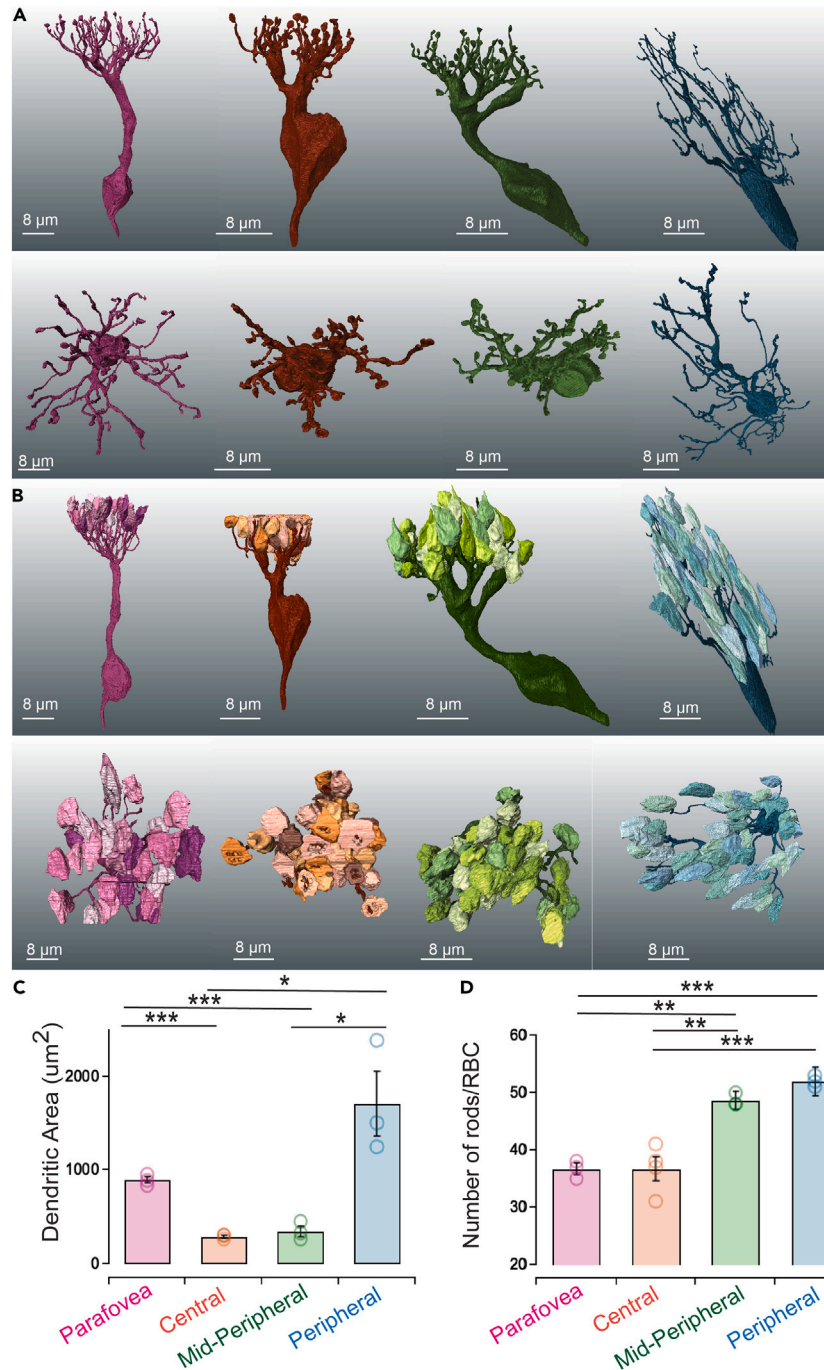


Figure 4. Rod convergence to rod bipolar cells across retinal eccentricities

(A) 3D reconstructions of rod bipolar cells (RBCs) that contact rod spherules at different locations of the macaque retina—parafovea (magenta), central (brown), mid-peripheral (green), and peripheral (blue). Top panel: side view of RBC soma and dendritic arbor; bottom panel: top-down view of RBC arbor.

(B) 3D rendering of all rod spherules contacting an individual RBC at different retinal locations—parafovea (magenta, rods in shades of pink), central (brown, rods in shades of orange), mid-peripheral (green, rods in lighter shades of green), and peripheral (blue, rods in lighter shades of blue) retina. Top panel: side view; bottom panel: top-down view. (Scale bar: 8 μm).

(C) Quantification of RBC dendritic arbor area across retinal regions. Parafovea: $894.36 \pm 32.13 \mu\text{m}^2$ (n = 3), central: $290.07 \pm 14.85 \mu\text{m}^2$ (n = 3), mid-periphery: $345.53 \pm 55.32 \mu\text{m}^2$ (n = 3), and periphery: $1714.17 \pm 343.10 \mu\text{m}^2$ (n = 3). The circles represent individual data points. n = number of RBCs reconstructed. Error bars represents mean \pm SEM. Statistics: Tukey's multiple comparison test was performed.

Figure 4. Continued

(D) Comparison of number of rods converging onto a single RBC across different locations of macaque retina. Parafovea: 34.67 ± 2.40 ($n = 3$), central: 36.50 ± 2.06 ($n = 4$), mid-periphery: 47.67 ± 0.33 ($n = 3$ RBCs), and periphery: 52 ± 0.58 ($n = 3$). The circles represent individual data points. n = number of RBCs reconstructed. Error bars represents mean \pm SEM. Statistics: Tukey's multiple comparison test was performed.

postsynaptic processes per rod terminal (Figure 3F; Table S3). The number of postsynaptic RBC processes has a greater variation across marmoset rod terminals than the number of postsynaptic HC processes. In fact, the most common scenario in marmoset rod spherules comprises six RBC postsynaptic processes, which is 2-fold greater than rod spherules in any location in macaque retina and 3-fold greater than those in mouse retina (Figure 3G; Table S3). In contrast, the most common number of HC processes for contacting marmoset rod spherules is similar or near similar to that in macaque and mouse retina (Figure 3H; Table S3). Overall, the increased divergence of postsynaptic processes seems to be unique to marmoset rod spherules. Taken together, our results demonstrate that rod synapses in mouse and marmoset retina exhibit significant differences in their synaptic organization which is correlated with the ratio of rod to cone density across species.

Convergence of rods to RBCs increases in a nonlinear manner from parafovea to periphery

Like divergence, another fundamental motif of synaptic connectivity is convergence, where a common postsynaptic neuron receives input from several presynaptic neurons.^{35–37} In the mammalian retina, rod-to-RBC connectivity demonstrates varying degrees of synaptic convergence based on species.^{21,38–40} Convergence plays an important role in controlling the efficacy with which single photon signals generated in the rods can be reliably discriminated from noise and hence relayed to the RBCs.^{41–43} For instance, in rabbit retina, rod convergence onto a single RBC is \sim 5-fold higher than that in mouse retina, and the threshold for separating signal and noise from the rod array in rabbit retina is quite different compared to the mouse retina.⁴³ To estimate rod convergence in primate retina across eccentricity, we reconstructed the entire dendritic arbor of multiple RBCs at each of the four retinal locations. We first estimated the area of the RBC dendritic arbor and found that the dendritic area and hence the morphology of the RBCs vary significantly across locations (Figures 4A and 4C). Peripheral RBCs have the largest dendritic field area followed by the parafoveal RBCs, whereas the mid-peripheral and central RBCs have much smaller dendritic areas. This was surprising, given previous reports that RBC dendritic areas could increase linearly toward the peripheral primate retina.²⁴ The fact that parafoveal RBC dendrites share a similar arborization pattern as peripheral RBCs is thus striking. The area of the RBC dendritic arbor thus follows the same pattern as the rod and RBC density across primate retinal locations, indicating that availability of space might serve as a primary constraint regulating the proliferation of RBC dendrites across retinal locations. Parafoveal RBCs also exhibit a unique dendritic morphology as they have a long primary arbor/central stalk before branching commences (Figure 4A, left). However, for RBCs in other locations, the primary dendrite branches soon after it exits the cell body.

Rod convergence (number of rods a single RBC pools from) did not necessarily scale with the size of the RBC dendritic area across retinal locations (Figures 4B and 4D). Although the rod convergence was highest for the peripheral RBCs, the estimate in the mid-peripheral retina, where RBC dendritic area is \sim 6-fold smaller, is quite close. Parafoveal and central RBCs exhibit near-equal rod convergence despite a 3-fold difference in the RBC dendritic area across these two locations. These results indicate that rod convergence does not change in a linear fashion with increasing distance from the fovea, nor does it follow the same trend as the rod density or RBC dendritic area across locations.

We next tested if our estimates of convergence and divergence agree with the following relationship of rod-to-RBC connectivity proposed in previous anatomical studies^{44,45}: $[\text{Rod density}] \times [\text{Divergence}] = [\text{RBC density}] \times [\text{Convergence}]$. We used published numbers of rod and RBC density from previous studies^{24,46} and used our measurements of divergence and convergence (Figures 2F and 4D). Our estimates of $[\text{RBC density}] \times [\text{Convergence}]$ exceeded that of $[\text{Rod density}] \times [\text{Divergence}]$ considerably at all locations (Table S4). This means that there are other factors such as dendritic overlap between neighboring RBCs and dendritic complexity which need to be considered in the above relationship to accurately estimate convergence or divergence.

Degree of overlap between neighboring RBCs and shared rod input across locations

We next determined the extent to which the dendritic arbors of neighboring RBCs overlap in the primate retina and how this spatial pattern could change across eccentricity. Retinal neurons exhibit a key design principle of spatial organization called “tiling” by which the dendrites of a particular neuron extend out to the dendritic tips of the neighboring neuron of the same subtype thereby minimizing dendritic overlap.^{29,47,48} Such a regular spatial distribution among retinal neurons is thought to be crucial for uniform sampling of the visual scene.⁴⁷ The dendritic arbors of most mammalian cone retinal bipolar cell types have been shown to exhibit tiling across the retinal space.²⁹ To assess tiling of neighboring primate RBCs across retinal regions, we reconstructed multiple adjacent RBCs at the four retinal locations and estimated their shared dendritic arbors (Figures 5A–5C). Neighboring RBCs at each retinal location exhibit considerable degree of overlap between their dendritic fields, with values as high as \sim 50% (Figure 5D). Dendrites of neighboring parafoveal RBCs exhibited the highest degree of overlap among all retinal locations. This suggests that unlike mammalian cone bipolar cells, primate RBC dendrites do not show tiling of the retinal space. Our results are also consistent with previous studies in mouse and human retina, which reported \sim 50% dendritic overlap between neighboring RBCs.^{32,49} The variability in the % overlap (5–50%) of nearby RBC dendritic arbors was also quite high at all retinal locations which could potentially result from the varying distance between reconstructed neighboring RBCs (Figure 5B).

We used another approach to quantify the dendritic overlap between neighboring RBCs by calculating the coverage factor⁴⁴ which is the product of RBC dendritic area, estimated in Figure 4C, with RBC density taken from a previous study.²⁴ The estimates of RBC coverage factors are as follows: parafovea - 4.5 ± 0.16 ; central - 3.5 ± 0.18 ; mid-periphery - 2.6 ± 0.41 ; periphery - 8.6 ± 1.7 . These results are overall consistent

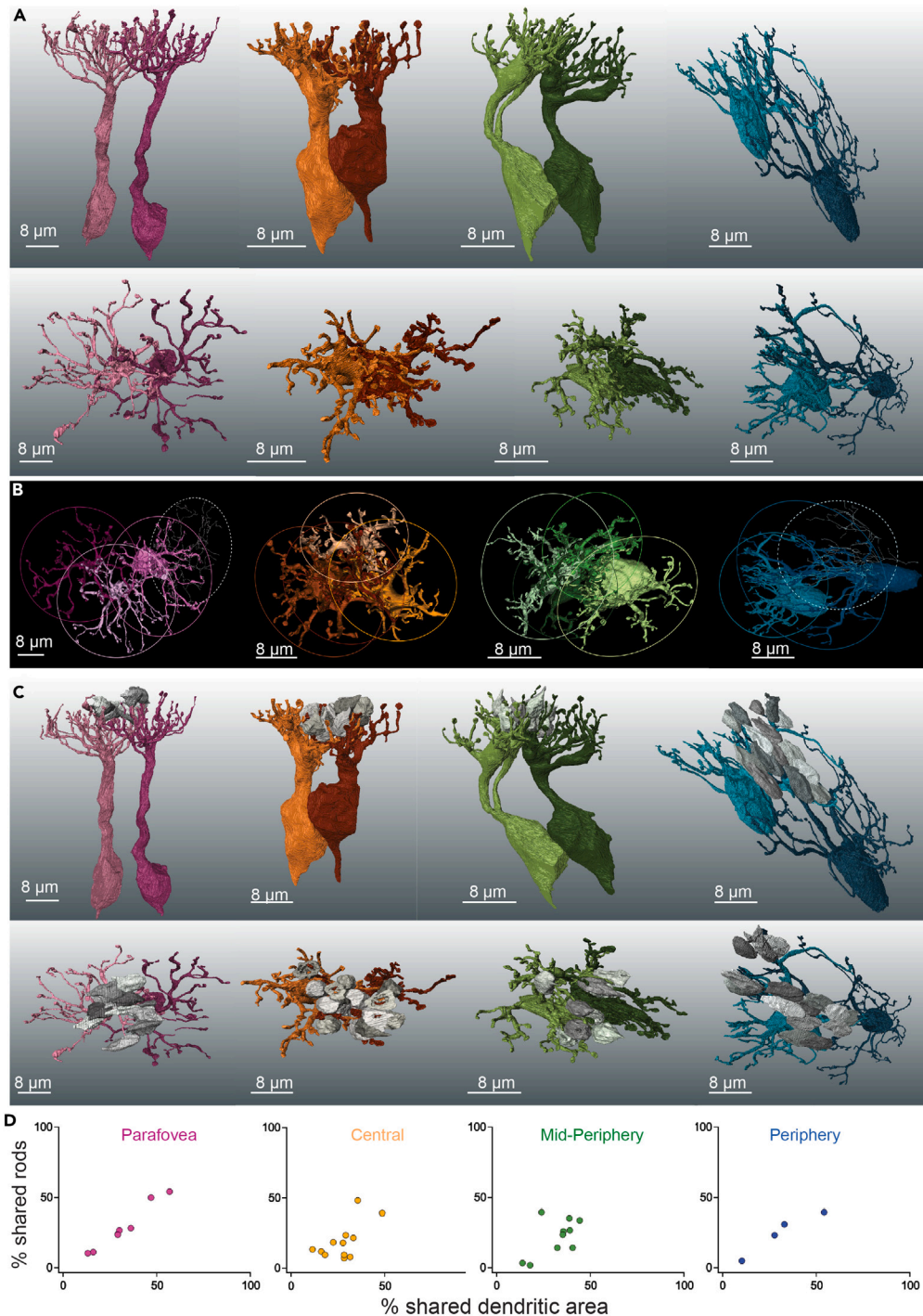


Figure 5. Overlap in rod connectivity and dendritic area between neighboring rod bipolar cells across retinal locations

(A) Dendritic arbor of two neighboring RBCs that share rod input across different regions of the primate retina. Side (top panels) and top-down (bottom panels) view of the 3D reconstructed profile of neighboring RBCs with overlapping dendritic arbors and sharing rod inputs in the parafovea (magenta), central (brown), mid-peripheral (green), and peripheral (blue) retina.

(B) Dendritic arbor overlaps between neighboring RBCs across different regions of the macaque retina. Each oval depicts the dendritic arbor of an individual RBC. The dendritic overlap has been estimated from the overlap between two ellipses.

(C) Side (top panels) and top-down (bottom panels) view of rods (in gray) shared between neighboring RBCs at the parafovea, central, mid-peripheral, and peripheral region of the macaque retina.

(D) Comparison of the fraction of rods shared per unit shared dendritic area between two neighboring RBCs at the different regions of interest in the macaque retina. Scale bar: 8 μm.

with estimates of RBC coverage factor in human retina⁴⁹ and support our aforementioned findings of a significant overlap of the dendritic arbor in neighboring RBCs. Coverage factor has also been described as an estimate of synaptic divergence, i.e., the average number of RBCs postsynaptic to individual rod.⁴⁵ The coverage factor values calculated earlier are overall comparable to our estimates of rod-to-RBC synaptic divergence, except in the peripheral retina (Figure 2F). This could be due to the more elaborate and spread-out dendritic arbor of peripheral RBCs compared to RBCs in other locations of the macaque retina.

We next estimated the number of shared rods between adjacent RBCs at the different retinal regions and found that RBCs in the parafovea have the highest number of shared rods (Figure 5C). This result is consistent with the higher % overlap of neighboring RBC dendritic arbors in the parafovea. As expected from the wide range of % dendritic overlap between neighboring RBCs, the number of shared rods between pairs of adjacent RBCs also varied substantially irrespective of the retinal location (Figure 5D). Neighboring parafoveal RBCs shared 4–19 rods, central RBCs shared 3–15 rods, mid-peripheral RBCs shared 1–17 rods, and peripheral RBCs shared 2–16 rods. To confirm that the % of dendritic overlap between adjacent RBCs is directly correlated with the % of shared rods, we calculated the number of shared rods per unit shared dendritic area for RBCs and found a positive correlation between the two parameters across all the retinal locations (Figure 5D). Taken together, our results show that neighboring RBCs in primate retina display a great amount of dendritic overlap and have a similar degree of information sharing with rods at all retinal locations.

DISCUSSION

It is well known that regional variation in the sensitivity of human daylight vision is largely driven by the differences in cone photoreceptor synapse and circuit organization across retinal eccentricity. Here we identify key regional differences in the fundamental organization and connectivity of the rod photoreceptor synapse—a critical juncture in the primate night vision pathway. The overall arrangement of the rod synapse with the postsynaptic RBC and HC is thought to be well conserved across mammals.^{9,18,20} In fact, a previous study in cat retina suggested that the rod synapse is largely invariant in its size, shape, and organization from mouse to man because the primary function of the rod synapse is conserved, i.e., to effectively transmit the presence or absence of a single photon signal.¹⁸ However, subsequent studies identified synaptic differences in macaque and human rods in comparison to cat retina.^{15,20} But, to what extent do differences exist in the rod synapse within the same primate retina across distinct locations has not been systematically analyzed and determined. By performing a comprehensive ultrastructural analysis of rod synapses at four distinct retinal locations in the same primate species, we found that the rod synapse changes its synaptic architecture and wiring with postsynaptic partners in a manner quite distinct from previously described regional changes for primate cone photoreceptor synapse.^{7,11} For instance, our results show that the rod synapse is more similar in its presynaptic organization and number of postsynaptic partners, between the parafoveal and the peripheral retina than the cone synapses are at these two locations. This may be because in contrast to a unidirectional steep decrease in cone density from the foveal center to the peripheral retina, there is first a steep increase in rod density from the parafovea to the central retina followed by a slow but steady decrease toward peripheral retina (Figure S1).^{9,46} This causes the rod and RBC density to be nearly similar in the parafoveal and peripheral retina even though the cone density differs by over 10-fold between these two locations.^{9,46} Such similarities in cellular density may also explain why central and mid-peripheral rod synapses are more alike than the other two locations. Despite the similarities, some of the differences in rod and RBC ribbon numbers and convergence between parafoveal and peripheral retina could be due to differences in the ratio of rod to cone density at these locations (Figure S1B). We further validated this idea of rod synapse organization and wiring being shaped by relative density of rods and cones by reconstructing the mouse and marmoset rod synapse and mapping the local circuitry (Figure 3). Mouse retina which has a high rod-to-cone density^{9,22} demonstrate patterns of rod synapse architecture and divergence most comparable to central and mid-peripheral macaque retina, whereas marmoset peripheral retina with a low rod-to-cone density shares features of rod synapses most comparable to parafoveal macaque retina.

Our results suggest that, barring a few, most facets of basic synaptic organization and connectivity of the rod to RBC, HC synapse change across retinal locations. This is unlike rod synapses in mouse and cat retina where there is little to no deviation in the synapse architecture and connectivity across the population.^{18,21} Moreover, unlike mouse retina, the dominant route for rod signal transmission in the primate retina is via the rod-to-RBC synapse; hence, changes in rod synaptic organization in the primate retina may have a bigger impact on downstream dim light signaling.⁵⁰ Therefore, regional changes in primate rod synapse can impact synaptic/circuit function and hence sensory processing in the night vision pathway. Early studies have suggested that based on the statistical variability of the synaptic neurotransmitter release process, mammalian rod ribbon synapses need to have a high tonic release rate in darkness to effectively signal the capture of a single photon.¹⁷ Such a small signal causes a small membrane hyperpolarization of rods, resulting in a brief reduction/pause in neurotransmitter release at the rod synapse. It has been proposed that on the presynaptic side having multiple ribbons or synaptic units per rod spherule could potentially increase this tonic release rate to better encode sparse dim light signals.^{17,18} On the postsynaptic side, when a single ribbon is opposed to four postsynaptic RBC and HC processes in a tight space, it allows the release of neurotransmitters to equally activate all four of the postsynaptic elements. Such a configuration has been proposed to be far more compact than having four separate release sites juxtaposed to four postsynaptic processes such as in hippocampal or cortical synaptic boutons.¹⁸ This means that with greater number of postsynaptic processes per rod spherule, the overall activation of the postsynaptic neuron is greater. In the macaque parafoveal and peripheral retina where rod density is low, having more ribbons and/or synaptic units per rod spherule compared to intermediate retinal locations with higher rod density could be a compensatory mechanism of the rod synapse to boost signal detection and signal transmission at these locations. Moreover, due to instances of higher ribbons and/or synaptic units in the parafoveal and peripheral rods, there is also a higher number of postsynaptic partners or synaptic divergence which allows further amplification and diversification of dim light signals. The high degree of synaptic divergence is

particularly striking in the marmoset peripheral rods which might suggest a greater need for maximizing signal transmission from individual rods to downstream RBCs and HCs than macaque retina.

Our results suggest that space availability in the retina might dictate the synaptic divergence and convergence patterns we observe across regions and species. For instance, lower rod density in the parafoveal and peripheral macaque retina and marmoset peripheral retina leads to more synaptic divergence per rod terminal to maximize information spread to the downstream circuitry from a single rod. In terms of convergence, the lower rod and RBC density in the parafoveal and peripheral retina may drive the expansion of the rod bipolar dendritic arbor area so that it can reach out to more rods and maximize convergence. Availability of space to make synaptic connections between rods and RBCs is further constrained by the relative packing of rods and cones in the photoreceptor sheet as well as the overlap in the dendritic area of neighboring RBCs. In fact, the coverage factor—a measure of dendritic overlap—is higher in parafoveal and peripheral RBCs than other locations which shows a compensatory mechanism in tiling of RBCs to facilitate an increase in synaptic divergence in regions of lower rod density. Conversely, in regions of higher rod density, synaptic divergence of rod to RBC is less, together with a smaller RBC coverage factor. In addition to density of rods and RBCs, dendritic complexity and branching of RBCs could further dictate the number of synaptic contacts with rods and hence convergence. For instance, central and mid-peripheral RBCs with similar dendritic area exhibit considerable differences in their rod convergence which is not proportionate to the difference in rod density between these two regions.

What is the functional impact of such regional variations in synaptic convergence between rod and RBCs? The near-identical rod convergence between parafoveal and central RBCs (Figure 4D) due to an increase in the dendritic field area of RBCs in the parafovea could be a strategy to equalize the dim light sensitivity of parafoveal RBCs with central RBCs at the cost of a coarser resolution. Mid-peripheral and peripheral RBCs due to higher convergence will have higher sensitivity and coarser resolution than parafoveal and central RBCs. Previous studies in peripheral primate retina have in fact shown a tight correlation between rod convergence and dim light sensitivity of the primary night vision pathway.^{43,51} Rod convergence is also important for the rod signals to be optimally filtered by pooling of inputs because the night vision pathway operates under conditions when photons are sparse and the rod signal-to-noise ratio is quite low.^{42,51,52} Hence, differences in rod convergence could shape how rod signals are integrated and optimally filtered. For instance, a lower degree of rod convergence in parafoveal and central RBCs would predict that the probability distribution across the smaller rod array is lower and hence the position of the nonlinear threshold to effectively separate the noise and single photon signal in rods should be placed at a lower value. However, in the case of peripheral RBCs which collect inputs from a larger pool of rods, the threshold instead will need to be placed at a higher value to effectively separate signal and noise.⁴¹ Hence, this could lead to regional differences in the sensitivity of RBCs and the downstream night vision circuitry. Thus, even though the central primate retina is specialized for high acuity daylight vision, we know that the dim light sensitivity of our averted vision, commonly used by stargazers to identify faint celestial objects in the night sky, peaks at a visual angle of $\sim 8\text{--}10^\circ$ ⁵³ which is in between what we define as parafoveal and central retina. Thus, in future studies it will be interesting to test the threshold of dim light detection of the primary night vision pathway in the primate retina at these central locations and compare how similar or dissimilar this is to peripheral retina.

Limitations of the study

A limitation of our study is not being able to directly relate the anatomical variations we observe in the rod synapse organization and connectivity across retinal locations to differences in synapse output and circuit function. This is because of challenges in targeting RBCs in primate retina for single-cell electrophysiological recordings. Unlike mouse retina, the soma of the RBCs in primate retina does not have a characteristic morphology or location in the inner nuclear layer that allows them to be distinguished from other bipolar cell types. Another limitation is the incomplete wiring pattern of the rods to HCs since HC processes extend over large area well beyond the 3D image volume that we reconstructed. This prevented us from estimating rod convergence onto single HCs similar to how we estimated that metric for RBCs in this study.

STAR★METHODS

Detailed methods are provided in the online version of this paper and include the following:

- KEY RESOURCES TABLE
- RESOURCE AVAILABILITY
 - Lead contact
 - Materials availability
 - Experimental model and study participant details
 - Data and code availability
- METHOD DETAILS
 - Tissue preparation and serial electron microscopy
 - Image segmentation and cell identification
- QUANTIFICATION AND STATISTICAL ANALYSIS

SUPPLEMENTAL INFORMATION

Supplemental information can be found online at <https://doi.org/10.1016/j.isci.2023.108113>.

ACKNOWLEDGMENTS

We thank the Wisconsin and Washington National Primate Research Centers for providing primate retinal tissue, R. Massey, J. Campbell, and the UW Madison SMPH EM facility for assistance with preparing samples and collecting the electron microscopy data. We also thank F. Rieke and M. Manookin for procurement of some of the tissue samples, S. Knecht and R. Wong for assistance with some of the serial electron microscopy image collection.

Funding: National Institutes of Health grant R01EY031411 (RS). McPherson Eye Research Institute's Rebecca Meyer Brown/Retina Research Foundation Professorship (MH), David and Nancy Walsh Professorship (RS). Wisconsin Partnership Program, University of Wisconsin School of Medicine and Public Health (RS). MH, UW2020 WARF Discovery award (MH, RS). Research to Prevent Blindness Inc. (MH, RS).

Data and materials availability: All data needed to evaluate the conclusions in the paper are present in the paper and/or the Supplementary Materials. Additional data related to this paper is available upon request from the Lead contact.

AUTHOR CONTRIBUTIONS

Conceptualization: RS, MH.

Methodology: RS, MH.

Investigation: AS, JZ, KM, HZ, PJD.

Visualization: AS, JZ, KM.

Supervision: RS, MH.

Writing—original draft: AS, KM, RS, MH.

Writing—review & editing: RS, MH.

DECLARATION OF INTERESTS

The authors declare they have no competing interests.

INCLUSION AND DIVERSITY

We support inclusive, diverse, and equitable conduct of research.

Received: March 22, 2023

Revised: August 25, 2023

Accepted: September 29, 2023

Published: October 2, 2023

REFERENCES

- Mullen, K.T. (1991). Colour vision as a post-receptoral specialization of the central visual field. *Vision Res.* 31, 119–130. [https://doi.org/10.1016/0042-6989\(91\)90079-k](https://doi.org/10.1016/0042-6989(91)90079-k).
- Noorlander, C., Koenderink, J.J., den Ouden, R.J., and Edens, B.W. (1983). Sensitivity to spatiotemporal colour contrast in the peripheral visual field. *Vision Res.* 23, 1–11. [https://doi.org/10.1016/0042-6989\(83\)90035-4](https://doi.org/10.1016/0042-6989(83)90035-4).
- Hecht, S., and Verrijp, C.D. (1933). The Influence of Intensity, Color and Retinal Location on the Fusion Frequency of Intermittent Illumination. *Proc. Natl. Acad. Sci. USA* 19, 522–535. <https://doi.org/10.1073/pnas.19.5.522>.
- Wässle, H., Grünert, U., Röhrenbeck, J., and Boycott, B.B. (1989). Cortical magnification factor and the ganglion cell density of the primate retina. *Nature* 341, 643–646. <https://doi.org/10.1038/341643a0>.
- Wikler, K.C., Williams, R.W., and Rakic, P. (1990). Photoreceptor mosaic: number and distribution of rods and cones in the rhesus monkey retina. *J. Comp. Neurol.* 297, 499–508. <https://doi.org/10.1002/cne.902970404>.
- Kolb, H., and Marshak, D. (2003). The midget pathways of the primate retina. *Doc. Ophthalmol.* 106, 67–81.
- Calkins, D.J., Schein, S.J., Tsukamoto, Y., and Sterling, P. (1994). M and L cones in macaque fovea connect to midget ganglion cells by different numbers of excitatory synapses. *Nature* 371, 70–72. <https://doi.org/10.1038/371070a0>.
- Sinha, R., Hoon, M., Baudin, J., Okawa, H., Wong, R.O.L., and Rieke, F. (2017). Cellular and Circuit Mechanisms Shaping the Perceptual Properties of the Primate Fovea. *Cell* 168, 413–426.e12. <https://doi.org/10.1016/j.cell.2017.01.005>.
- Grünert, U., and Martin, P.R. (2020). Cell types and cell circuits in human and non-human primate retina. *Prog. Retin. Eye Res.* 78, 100844. <https://doi.org/10.1016/j.preteyeres.2020.100844>.
- Curcio, C.A., Sloan, K.R., Kalina, R.E., and Hendrickson, A.E. (1990). Human photoreceptor topography. *J. Comp. Neurol.* 292, 497–523. <https://doi.org/10.1002/cne.902920402>.
- Chun, M.H., Grünert, U., Martin, P.R., and Wässle, H. (1996). The synaptic complex of cones in the fovea and in the periphery of the macaque monkey retina. *Vision Res.* 36, 3383–3395. [https://doi.org/10.1016/0042-6989\(95\)00334-7](https://doi.org/10.1016/0042-6989(95)00334-7).
- Lagnado, L., and Schmitz, F. (2015). Ribbon Synapses and Visual Processing in the Retina. *Annu. Rev. Vis. Sci.* 1, 235–262. <https://doi.org/10.1146/annurev-vision-082114-035709>.
- Sjostrand, F.S. (1958). Ultrastructure of retinal rod synapses of the guinea pig eye as revealed by three-dimensional reconstructions from serial sections. *J. Ultrastruct. Res.* 2, 122–170. [https://doi.org/10.1016/s0022-5320\(58\)90050-9](https://doi.org/10.1016/s0022-5320(58)90050-9).
- Missotten, L. (1960). [A study of the rods of the human retina by means of the electron microscope]. *Ophthalmologica* 140, 200–214. <https://doi.org/10.1159/000303831>.
- Tsukamoto, Y., and Omi, N. (2022). Multiple Invagination Patterns and Synaptic Efficacy in Primate and Mouse Rod Synaptic Terminals. *Invest. Ophthalmol. Vis. Sci.* 63, 11. <https://doi.org/10.1167/iov.63.8.11>.
- Missotten, L. (1965). *The Ultrastructure of the Retina* (Editions Arscia SA).
- Rao, R., Buchsbaum, G., and Sterling, P. (1994). Rate of quantal transmitter release at the mammalian rod synapse. *Biophys. J.* 67, 57–63. [https://doi.org/10.1016/S0006-3495\(94\)80454-0](https://doi.org/10.1016/S0006-3495(94)80454-0).
- Rao-Mirotnik, R., Harkins, A.B., Buchsbaum, G., and Sterling, P. (1995). Mammalian rod terminal: architecture of a binary synapse. *Neuron* 14, 561–569. [https://doi.org/10.1016/0896-6273\(95\)90312-7](https://doi.org/10.1016/0896-6273(95)90312-7).
- Matthews, G., and Fuchs, P. (2010). The diverse roles of ribbon synapses in sensory

- neurotransmission. *Nat. Rev. Neurosci.* 11, 812–822. <https://doi.org/10.1038/nrn2924>.
20. Migdale, K., Herr, S., Klug, K., Ahmad, K., Linberg, K., Sterling, P., and Schein, S. (2003). Two ribbon synaptic units in rod photoreceptors of macaque, human, and cat. *J. Comp. Neurol.* 455, 100–112. <https://doi.org/10.1002/cne.10501>.
21. Tsukamoto, Y., and Omi, N. (2013). Functional allocation of synaptic contacts in microcircuits from rods via rod bipolar to All amacrine cells in the mouse retina. *J. Comp. Neurol.* 521, 3541–3555. <https://doi.org/10.1002/cne.23370>.
22. Jeon, C.J., Strettoi, E., and Masland, R.H. (1998). The major cell populations of the mouse retina. *J. Neurosci.* 18, 8936–8946. <https://doi.org/10.1523/JNEUROSCI.18-21-08936.1998>.
23. Wilder, H.D., Grünert, U., Lee, B.B., and Martin, P.R. (1996). Topography of ganglion cells and photoreceptors in the retina of a New World monkey: the marmoset *Callithrix jacchus*. *Vis. Neurosci.* 13, 335–352. <https://doi.org/10.1017/s095252380007586>.
24. Grünert, U., and Martin, P.R. (1991). Rod bipolar cells in the macaque monkey retina: immunoreactivity and connectivity. *J. Neurosci.* 11, 2742–2758. <https://doi.org/10.1523/JNEUROSCI.11-09-02742.1991>.
25. Gamlin, C.R., Zhang, C., Dyer, M.A., and Wong, R.O.L. (2020). Distinct Developmental Mechanisms Act Independently to Shape Biased Synaptic Divergence from an Inhibitory Neuron. *Curr. Biol.* 30, 1258–1268.e2. <https://doi.org/10.1016/j.cub.2020.01.080>.
26. Kazama, H., and Wilson, R.I. (2009). Origins of correlated activity in an olfactory circuit. *Nat. Neurosci.* 12, 1136–1144. <https://doi.org/10.1038/nn.2376>.
27. Toth, K., Soares, G., Lawrence, J.J., Philips-Tansey, E., and McBain, C.J. (2000). Differential mechanisms of transmission at three types of mossy fiber synapse. *J. Neurosci.* 20, 8279–8289. <https://doi.org/10.1523/JNEUROSCI.20-22-08279.2000>.
28. Asari, H., and Meister, M. (2012). Divergence of visual channels in the inner retina. *Nat. Neurosci.* 15, 1581–1589.
29. Wässle, H., Puller, C., Müller, F., and Haverkamp, S. (2009). Cone contacts, mosaics, and territories of bipolar cells in the mouse retina. *J. Neurosci.* 29, 106–117. <https://doi.org/10.1523/JNEUROSCI.4442-08.2009>.
30. Euler, T., Haverkamp, S., Schubert, T., and Baden, T. (2014). Retinal bipolar cells: elementary building blocks of vision. *Nat. Rev. Neurosci.* 15, 507–519. <https://doi.org/10.1038/nrn3783>.
31. Cohen, E., and Sterling, P. (1990). Convergence and divergence of cones onto bipolar cells in the central area of cat retina. *Philos. Trans. R. Soc. Lond. B Biol. Sci.* 330, 323–328. <https://doi.org/10.1098/rstb.1990.0202>.
32. Behrens, C., Schubert, T., Haverkamp, S., Euler, T., and Berens, P. (2016). Connectivity map of bipolar cells and photoreceptors in the mouse retina. *Elife* 5, e20041. <https://doi.org/10.7554/eLife.20041>.
33. Grabner, C.P., Gandini, M.A., Rehak, R., Le, Y., Zamponi, G.W., and Schmitz, F. (2015). RIM1/2-Mediated Facilitation of Cav1.4 Channel Opening Is Required for Ca²⁺-Stimulated Release in Mouse Rod Photoreceptors. *J. Neurosci.* 35, 13133–13147. <https://doi.org/10.1523/JNEUROSCI.0658-15.2015>.
34. Hagiwara, A., Kitahara, Y., Grabner, C.P., Vogl, C., Abe, M., Kitta, R., Ohta, K., Nakamura, K., Sakimura, K., Moser, T., et al. (2018). Cytomatrix proteins CAST and ELKS regulate retinal photoreceptor development and maintenance. *J. Cell Biol.* 217, 3993–4006. <https://doi.org/10.1083/jcb.201704076>.
35. Hoon, M., Okawa, H., Della Santina, L., and Wong, R.O.L. (2014). Functional architecture of the retina: Development and disease. *Prog. Retin. Eye Res.* 42, 44–84.
36. Mombaerts, P. (2006). Axonal wiring in the mouse olfactory system. *Annu. Rev. Cell Dev. Biol.* 22, 713–737. <https://doi.org/10.1146/annurev.cellbio.21.012804.093915>.
37. Huang, C.C., Sugino, K., Shima, Y., Guo, C., Bai, S., Mensh, B.D., Nelson, S.B., and Hantman, A.W. (2013). Convergence of pontine and proprioceptive streams onto multimodal cerebellar granule cells. *Elife* 2, e00400. <https://doi.org/10.7554/eLife.00400>.
38. Li, W., Keung, J.W., and Massey, S.C. (2004). Direct synaptic connections between rods and OFF cone bipolar cells in the rabbit retina. *J. Comp. Neurol.* 474, 1–12. <https://doi.org/10.1002/cne.20075>.
39. Protti, D.A., Flores-Herr, N., Li, W., Massey, S.C., and Wässle, H. (2005). Light signaling in scotopic conditions in the rabbit, mouse and rat retina: a physiological and anatomical study. *J. Neurophysiol.* 93, 3479–3488. <https://doi.org/10.1152/jn.00839.2004>.
40. Bloomfield, S.A., and Dacheux, R.F. (2001). Rod vision: pathways and processing in the mammalian retina. *Prog. Retin. Eye Res.* 20, 351–384. [https://doi.org/10.1016/s1350-9462\(00\)00031-8](https://doi.org/10.1016/s1350-9462(00)00031-8).
41. Pahlberg, J., and Sampath, A.P. (2011). Visual threshold is set by linear and nonlinear mechanisms in the retina that mitigate noise: how neural circuits in the retina improve the signal-to-noise ratio of the single-photon response. *Bioessays* 33, 438–447. <https://doi.org/10.1002/bies.201100014>.
42. Field, G.D., and Sampath, A.P. (2017). Behavioural and physiological limits to vision in mammals. *Philos. Trans. R. Soc. Lond. B Biol. Sci.* 372, 20160072. <https://doi.org/10.1098/rstb.2016.0072>.
43. Trexler, E.B., Casti, A.R.R., and Zhang, Y. (2011). Nonlinearity and noise at the rod-rod bipolar cell synapse. *Vis. Neurosci.* 28, 61–68. <https://doi.org/10.1017/S0952523810000301>.
44. Wässle, H., Peichl, L., and Boycott, B.B. (1981). Dendritic territories of cat retinal ganglion cells. *Nature* 292, 344–345. <https://doi.org/10.1038/292344a0>.
45. Freed, M.A., Smith, R.G., and Sterling, P. (1987). Rod bipolar array in the cat retina: pattern of input from rods and GABA-accumulating amacrine cells. *J. Comp. Neurol.* 266, 445–455. <https://doi.org/10.1002/cne.902660310>.
46. Packer, O., Hendrickson, A.E., and Curcio, C.A. (1989). Photoreceptor topography of the retina in the adult pigtail macaque (*Macaca nemestrina*). *J. Comp. Neurol.* 288, 165–183. <https://doi.org/10.1002/cne.902880113>.
47. Masland, R.H. (2012). The neuronal organization of the retina. *Neuron* 76, 266–280. <https://doi.org/10.1016/j.neuron.2012.10.002>.
48. Lee, S.C.S., Cowgill, E.J., Al-Nabulsi, A., Quinn, E.J., Evans, S.M., and Reese, B.E. (2011). Homotypic regulation of neuronal morphology and connectivity in the mouse retina. *J. Neurosci.* 31, 14126–14133. <https://doi.org/10.1523/JNEUROSCI.2844-11.2011>.
49. Lee, S.C.S., Martin, P.R., and Grünert, U. (2019). Topography of Neurons in the Rod Pathway of Human Retina. *Invest. Ophthalmol. Vis. Sci.* 60, 2848–2859. <https://doi.org/10.1167/iovs.19-27217>.
50. Grimes, W.N., Baudin, J., Azevedo, A.W., and Rieke, F. (2018). Range, routing and kinetics of rod signaling in primate retina. *Elife* 7, e38281. <https://doi.org/10.7554/eLife.38281>.
51. Field, G.D., and Rieke, F. (2002). Nonlinear signal transfer from mouse rods to bipolar cells and implications for visual sensitivity. *Neuron* 34, 773–785. [https://doi.org/10.1016/s0896-6273\(02\)00700-6](https://doi.org/10.1016/s0896-6273(02)00700-6).
52. Dunn, F.A., Doan, T., Sampath, A.P., and Rieke, F. (2006). Controlling the gain of rod-mediated signals in the Mammalian retina. *J. Neurosci.* 26, 3959–3970. <https://doi.org/10.1523/JNEUROSCI.5148-05.2006>.
53. Alexander, R.G., Mintz, R.J., Custodio, P.J., Macknik, S.L., Vaziri, A., Venkatakrisnan, A., Gindina, S., and Martinez-Conde, S. (2021). Gaze mechanisms enabling the detection of faint stars in the night sky. *Eur. J. Neurosci.* 54, 5357–5367. <https://doi.org/10.1111/ejn.15335>.
54. Zhang, C., Hellevik, A., Takeuchi, S., and Wong, R.O. (2022). Hierarchical partner selection shapes rod-cone pathway specificity in the inner retina. *iScience* 25, 105032. <https://doi.org/10.1016/j.isci.2022.105032>.
55. Abbott, C.J., Percival, K.A., Martin, P.R., and Grünert, U. (2012). Amacrine and bipolar inputs to midget and parasol ganglion cells in marmoset retina. *Vis. Neurosci.* 29, 157–168.
56. Zhang, C., Kim, Y.J., Silverstein, A.R., Hoshino, A., Reh, T.A., Dacey, D.M., and Wong, R.O. (2020). Circuit Reorganization Shapes the Developing Human Foveal Midget Connecome toward Single-Cone Resolution. *Neuron* 108, 905–918.e3. <https://doi.org/10.1016/j.neuron.2020.09.014>.
57. Rolls, E.T., and Cowey, A. (1970). Topography of the retina and striate cortex and its relationship to visual acuity in rhesus monkeys and squirrel monkeys. *Exp. Brain Res.* 10, 298–310. <https://doi.org/10.1007/BF00235053>.
58. Della Santina, L., Kuo, S.P., Yoshimatsu, T., Okawa, H., Suzuki, S.C., Hoon, M., Tsuboyama, K., Rieke, F., and Wong, R.O.L. (2016). Glutamatergic Monopolar Interneurons Provide a Novel Pathway of Excitation in the Mouse Retina. *Curr. Biol.* 26, 2070–2077. <https://doi.org/10.1016/j.cub.2016.06.016>.
59. Cardona, A., Saalfeld, S., Schindelin, J., Arganda-Carreras, I., Preibisch, S., Longair, M., Tomancak, P., Hartenstein, V., and Douglas, R.J. (2012). TrakEM2 software for neural circuit reconstruction. *PLoS One* 7, e38011. <https://doi.org/10.1371/journal.pone.0038011>.

STAR★METHODS

KEY RESOURCES TABLE

REAGENT or RESOURCE	SOURCE	IDENTIFIER
Biological samples		
Macaque retina	Regional Primate Research Center	N/A
Marmoset retina	Regional Primate Research Center	N/A
Mouse: C57/BL6	Jackson Laboratory	Strain #: 000664 RRID: MGI:6111814
Software and algorithms		
IGOR Pro	WaveMetrics	RRID: SCR_000325
Fiji	NIH	RRID: SCR_002285
Amira	ThermoFisher Scientific	RRID: SCR_014305
Biorender	BioRender.com	RRID: SCR_018361
Trak-EM2	Cardona et al.	RRID: SCR_008954
MATLAB	Mathworks	RRID: SCR_001622

RESOURCE AVAILABILITY

Lead contact

Further information and requests for resources and reagents should be directed to and will be fulfilled by the Lead Contact, Raunak Sinha (raunak.sinha@wisc.edu).

Materials availability

This study did not generate unique reagents.

Experimental model and study participant details

Primate retinal tissue was obtained from two adult (2 years and 7 years old respectively) male *Macaca nemestrina* (macaque) and an adult (7 years old) female *Callithrix jacchus* (marmoset) through the Tissue Distribution Programs at the Washington and Wisconsin National Primate Centers. Mouse retinal tissue was obtained from an adult (~ postnatal day 60) male C57/BL6 mouse. Rod synapse organization and connectivity in macaque, marmoset and C57/BL6 mouse retina as analyzed in this study, are not expected to exhibit sex-based differences.^{15,23,24,54,55} All procedures were approved by the Institutional Animal Care and Use Committee at the University of Wisconsin-Madison and the University of Washington.

Data and code availability

- The EM datasets used in the current study have not been deposited in a public repository because of the size of the datasets and use in ongoing studies but are available from the [lead contact](#) upon request.
- This paper does not report original code.
- Any additional information required to analyze data reported in the paper is available from the [lead contact](#) upon request.

METHOD DETAILS

Tissue preparation and serial electron microscopy

For the macaque, marmoset and mouse preparations, the retina was dissected in bicarbonate Ames solution. For the macaque retina preparation, the foveal center was identified as previously described.⁵⁶ In brief, we prepared samples for each retinal region for SBEM, by identifying the dimple-like appearance of the foveal pit/center in the temporal retina under a stereomicroscope. Four retinal regions were then cut out in temporal retina with increasing eccentricity from the foveal pit and prepared for electron microscopy. These regions were: parafoveal (~1 mm from the foveal pit/center), central (~3 mm from the foveal pit/center), mid-peripheral (~5 mm from the foveal pit/center) and peripheral (~10 mm from the foveal pit/center). 1 degree of visual angle in macaque corresponds to 0.246 mm.^{6,57} For the marmoset and mouse retina, the peripheral retina region was used. For the marmoset, this region was ~5 mm from the foveal pit (center). Retinas were immersion fixed in 4% glutaraldehyde in 0.1 M sodium cacodylate buffer (pH 7.4). Retinas were then washed in cacodylate buffer, stained, dehydrated, and embedded in Durcupan resin using an established protocol.⁵⁸

All retinas were sectioned and imaged across the vertical axis (cross-section). A Zeiss 3View Serial block face scanning electron microscope was used to section and image the retinal blocs. Image collection was optimized to visualize synaptic ribbons within photoreceptor terminals. For the macaque and mouse image stacks, a resolution of 5 nm/pixel was used. For the marmoset image stack a resolution of 6 nm/pixel was used. All stacks were acquired with a section thickness of 50 nm. Multi-montage acquisition was performed to capture wide field of views. Imaging was localized to the outer plexiform layer where photoreceptor terminals laminate and the inner nuclear layer where somas of rod bipolar cells and horizontal cells reside. Each tile of the montage was $\sim 45 \mu\text{m}$ in size.

Image segmentation and cell identification

Image stacks were imported, aligned and stitched using the TrakEM2 module in FIJI/ImageJ (NIH).⁵⁹ Rod photoreceptor terminals/spherules were identified by their stereotypic features as previously described.^{18,20,21} Electron dense ribbon structures within rod terminals were localized apposed to typical invaginating contacts as shown previously.^{20,21} Presence of ribbons were confirmed when the electron dense structure continued for at least 4 consecutive planes, close to the triad arrangement at the rod axon terminal. The rod bipolar cells (RBCs) were identified by following the central invaginating element into the rod spherule at the outer plexiform layer and following the processes till their somas at the inner nuclear layer. The 3D visualization of the RBC annotation showed the typical morphology of RBCs as detailed in previous studies.²¹ Rod spherules, RBC processes and HC processes were traced manually using the *AreaTree* function of TrakEM2. Ribbon synapses were annotated using *AreaList* function in TrakEM2. These annotations were subsequently visualized in Amira 2.0 (ThermoFisher Scientific). At each location of the macaque retina, at least 3 RBCs and all the rods contacting each RBC (approximately 100 rods per region) were reconstructed. For the mouse and marmoset peripheral retina, 50 and 22 rod spherules were reconstructed respectively.

QUANTIFICATION AND STATISTICAL ANALYSIS

We define synaptic units as ribbon synapses or part of a ribbon synapse juxtaposed to a distinct set of postsynaptic processes. On the presynaptic side, a synaptic unit can be the entire ribbon or part of a ribbon each of which lasts for at least 4 consecutive planes. On the postsynaptic side, each synaptic unit contacted a unique set of postsynaptic partners comprising of at least one distinct central or lateral element. For each rod spherule, we counted the number of synaptic units per ribbon and total number of synaptic units per rod spherule (Figure 1D). We traced back most of the RBC dendrites to their respective somas and did not observe instances of multiple RBC dendrites from the same rod spherule tracing back to the same RBC. Occasionally, one of the multiple dendrites of the RBCs at the rod spherules at the edge of the EM stacks could not be traced back to their somas since they were cut off from the stack. But we were able to trace the dendrites of the other RBCs and found that each dendritic invagination in the rod spherule is from a distinct RBC across locations. Processes of horizontal cells are much longer and extended beyond the image volume which was a limitation (as mentioned above) in tracing them back to their somas.

The dendritic area of RBC (Figures 4C and 5D) was calculated by drawing a polygon around the dendritic arbor of a specific RBC in FIJI and calculating the area of the polygon. To calculate the percentage of dendritic overlap, we drew a polygon around the dendritic arbor of an RBC and the overlapping section with a second neighboring RBC in a top-down 3D view. The percentage overlap was calculated by dividing the area of the polygon shared between the two RBCs by the area of the polygon encompassing the full dendritic arbor of the RBC (Figures 5B and 5D). In the parafoveal and peripheral stacks, for two RBCs (one in each stack, marked by dotted lines in Figure 5B), the complete dendritic arbor was not part of the acquired image stacks. However, based on the 3D renderings of these RBCs, the overlapping region with neighboring RBC was completely within the stack and has been used for quantifications of dendritic arbor overlap in Figure 5D. However, these RBCs have not been used for quantifying rod convergence (Figure 4D).

In Figures 1, 2, 3, and 4 the bar plots represent mean \pm SEM. For Figures 1, 2, and 3, the circles represent the relative frequency of occurrence of rod spherules or ribbons exhibiting distinct features with respect to the total number of rod spherules/ribbons quantified. The symbol size was set as a function of the weight of the parameter. The minimum and maximum sizes were then set to be 1 and the total number of instances quantified.

Tukey's multiple comparison tests were used to determine the statistical differences across regions in macaque retina (Figures 1, 2, and 4). An unpaired, two-tailed student's t-test was used to determine the statistical significance between rod spherules in mouse and marmoset retina (Figure 3). * = $p < 0.05$; ** = $p < 0.01$; *** = $p < 0.001$.